Ionic Liquid Containing Microemulsions: Probe by Conductance, Dynamic Light Scattering, Diffusion-Ordered Spectroscopy NMR Measurements, and Study of Solvent Relaxation Dynamics

ARTICLE *in* THE JOURNAL OF PHYSICAL CHEMISTRY B · FEBRUARY 2011

Impact Factor: 3.3 · DOI: 10.1021/jp110896w · Source: PubMed

THE JOURNAL OF PHYSICAL CHEMISTRY B

ARTICLE

pubs.acs.org/JPCB

Ionic Liquid Containing Microemulsions: Probe by Conductance, Dynamic Light Scattering, Diffusion-Ordered Spectroscopy NMR Measurements, and Study of Solvent Relaxation Dynamics

Rajib Pramanik, Souravi Sarkar, Chiranjib Ghatak, Vishal Govind Rao, and Nilmoni Sarkar*

Department of Chemistry, Indian Institute of Technology, Kharagpur 721302, WB, India

ABSTRACT: Room-temperature ionic liquid (RTIL), *N*-methyl-*N*-propylpyrrolidinium bis(trifluoromethanesulfonyl)imide ($[P_{13}][Tf_2N]$), was substituted for polar water and formed nonaqueous microemulsions with benzene by the aid of nonionic surfactant TX-100. The phase behavior of the ternary system was investigated, and microregions of $[P_{13}][Tf_2N]$-in-benzene (IL/O), bicontinuous, and benzene-in-$[P_{13}][Tf_2N]$ (O/IL) were identified by traditional electrical conductivity measurements. Dynamic light scattering (DLS) revealed the formation of these IL microemulsions because with gradual increase of RTIL contents the droplet sizes of the microemulsions are also gradually increasing. Pulsed-field gradient spin−echo NMR have been studied to measure the diffusion coefficients of neat $[P_{13}][Tf_2N]$ and $[P_{13}][Tf_2N]$ in microemulsions which indicate ionic liquid containing microemulsions is formed. Moreover, the dynamics of solvent relaxation have been investigated in $[P_{13}][Tf_2N]$/TX100/benzene microemulsions using steady-state and time-resolved fluorescence spectroscopy using coumarin 153 (C-153) and coumarin 480 (C-480) fluorescence probe with variation of RTIL contents in microemulsions. For both of the probes with increasing amount of ionic liquids in microemulsions the relative contribution of the fast components increases and the slow components contribution decreases; therefore the average solvation time decreases.

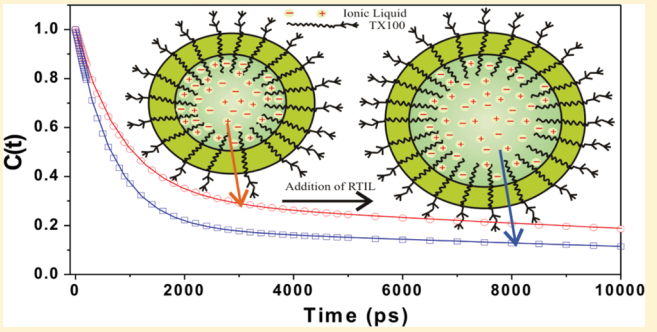

1. INTRODUCTION

In recent years room-temperature ionic liquids (RTILs) consisting of bulky cations paired with a variety of different anions have gained wide popularity because of their unique properties and wide range of applications. RTILs are characterized by low melting points, negligible vapor pressure, considerable polarity, wide liquid range, enhanced thermal stability, miscibility with other solvents, nonflammability, and chemical stability, particularly in the presence of air and moisture.[1−6] These properties have made RTILs better and environment-friendly reaction media in the chemical industry for extraction and fractionations,[7] material preparation,[8,9] synthesis, catalysis, and a host of other applications.[10,11]

Microemulsions are thermodynamically stable media formed by two and more immiscible liquids which are stabilized by surfactants. These microheterogeneous systems can solubilized both polar and nonpolar substances, and they have been applied to many fields, such as for chemical reaction, in material science, and in pharmaceutical industry.[12] The structure of microemulsions is a field of current interest. To study ionic liquid microemulsions, it is necessary to investigate the microemulsions structures. Conductivity is frequently used to investigate the structure and structural changes in microemulsions on the basis of percolation theory. The swelling behavior of microemulsions was detected by dynamics light scattering (DLS). Regular swelling behavior was obtained which is also in accordance with water-in-oil (W/O) type microemulsions. This result indicates ionic liquid microemulsion systems behave similarly to the traditional aqueous ones. Recently several groups prepared and characterized RTILs containing micelles and microemulsions.[13−17]

Recently, many photophysical studies have been undertaken in RTILs. Aki et al.[18] determined the polarity of imidazolium- and pyridinium-based RTILs using absorption and fluorescence spectroscopy. Muldoon et al.[19] estimated the polarity of RTILs using solvatochromic probes. Recently Reichardt showed how to determine the polarity of RTILs by means of solvatochromic betaine dyes.[20] Carmichael and Seddon[21] determined the polarity of several neat 1-alkyl-3-methylimidazolium-based RTILs using nile red as solvatochromic probe. Pyrene, betaine dye, nile red, and dansylamide have been used to probe RTIL−solvent mixtures.[22,23] The change in viscosity of RTILs with addition to different solvents is also investigated.[24,25] Photoisomerization of DODCI (3,3-diethyloxadicarbocyanine iodide) is also investigated in neat RTIL and RTIL−water mixture.[26] Recently Santhosh et al.[27,28] investigated excited-state intramolecular electron-transfer reaction and fluorescence response of 4-(*N*,*N*-dimethylamino)benzonitrile in RTILs by means of time-resolved fluorescence and multiphoton confocal microscopic study. The

Received: November 15, 2010
Revised: January 20, 2011
Published: February 22, 2011

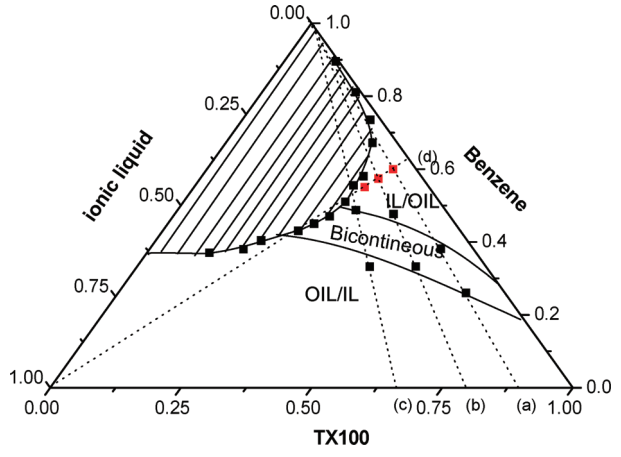

Figure 1. Phase diagram of the $[P_{13}][Tf_2N]$/TX100/benzene three-component system at 25 °C. For lines a, b, and c, the initial RTIL weight fraction are I = 0.10, 0.20, and 0.33 respectively.

solvent relaxation in different neat RTILs is also reported.[29−39] Solvation dynamics in a RTIL occurs in a slow nanosecond time scale along with a sub-picosecond component.[40,41] To understand the solvation process in RTILs, several groups carried out computer simulations on the structure and dynamics in a RTIL.[42] These simulations suggest that solvation dynamics in a RTIL involves collective motion of the cation and the anion.[42] The solvation dynamics has also been studied in the mixtures of RTILs and conventional solvents.[43−45] Adhikari et al.[46] investigated the dynamics in different regions of the 1-pentyl-3-methylimidazolium tetrafluoroborate ([pmim][BF_4]) containing microemulsions and also in neat [pmim][BF_4]. Petrich and co-workers studied solvation dynamics of coumarin 153 in amphiphilic ionic liquids, (1-cetyl-3-vinyl-imidazolium) bromide and 1-cetyl-3-vinyl-imidazolium bis(trifluoromethylsulfonyl)imide, and their micelles in water.[47] They suggested that the imidazolium moiety is responsible for the major part of the solvation dynamics.[47] The excitation wavelength dependent fluorescence behavior of some dipolar molecules in RTILs was investigated by Mandal et al.[48] which is attributed to the unusual red edge effect in RTILs. Recently Hu and Margulis[49] predicted the heterogeneity in RTILs and also observed the red edge effect in RTILs using molecular dynamics simulation.

In the present article, we have used nonionic surfactant TX100 as surfactant. The ternary phase diagram of the $[P_{13}][Tf_2N]$/TX100/benzene system [$[P_{13}][Tf_2N]$ = *N*-methyl-*N*-propylpyrrolidinium bis(trifluoromethanesulfonyl)imide] determined at 25 °C by direct observation is illustrated in Figure 1. We have also studied the formation of the microemulsions using dynamic light scattering, and also using a fluorescence probe, coumarin 480 (C480) and coumarin 153 (C153). Moreover, we have investigated the solvent relaxation dynamics in this microemulsions using TCSPC with time resolution of 90 ps. The structures of $[P_{13}][Tf_2N]$, C-480, and C-153 are shown in Scheme 1.

2. EXPERIMENTAL SECTION

C-480 and C153 (laser grade, Exciton) were used as received. $[P_{13}][Tf_2N]$ was obtained from Kanto Chemicals. TX-100 was purchased from Aldrich, and benzene was obtained from Spectrochem (UV spectroscopy grade). $[P_{13}][Tf_2N]$ and TX-100 were dried in a vacuum oven for 12 h at 70−80 °C before use. A

Scheme 1. Structures of RTIL, C-480 ,and C-153

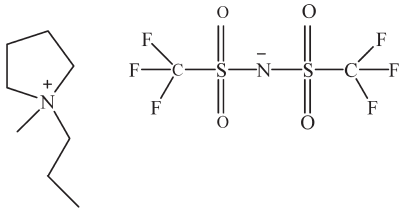

N-methyl-N-propyl bis(trifluoromethanesulfonyl) imide $[P_{13}][Tf_2N]$

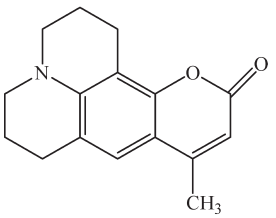

Coumarin-480

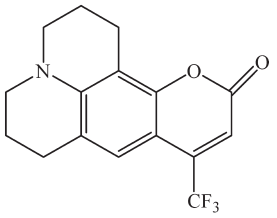

Coumarin-153

stock solution of 0.5 M TX100 in benzene was prepared at room temperature (25 °C) by direct weighting. We used this 0.5 M solution for all of the measurements. The RTIL content of the microemulsions solution (R value) was expressed by the molar ratio of added RTIL to surfactant (TX100); i.e., R value = (amount of RTIL in molar unit)/(amount of TX100 in molar unit). We made the solution transparent by gently shaking by hand. Different sizes of microemulsions were prepared by varying the molar ratio (R) of RTIL/TX-100. The final concentrations of TX100 and the probe in all experiments were kept at 0.5 and 10^{-5} M, respectively. All experiments were carried out at 25 °C.

The absorption and fluorescence spectra were measured using Shimadzu (model no. UV-2450) spectrophotometer and Hitachi F-7000 fluorescence spectrophotometer. For steady-state experiments, all samples were excited at 408 nm. The details of the time-resolved fluorescence setup are described elsewhere.[50] In brief, the samples were excited at 408 nm using a picosecond laser diode (IBH, Nanoled), and the signals were collected at the magic angle (54.7°) using a Hamamatsu microchannel plate photomultiplier tube (3809U). The instrument response function of our setup was 90 ps. The analysis of the data was done using IBH DAS, version 6 decay analysis software. All of the longer and shorter wavelength decays were fitted with biexponential and triexponential functions, respectively, because χ^2 becomes closer to 1, which indicates a good fit. For DLS measurements, we used a Malvern Nano ZS instrument employing a 4 mW He−Ne laser (λ = 632.8 nm). All of the scattering photons were collected at a 173° scattering angle. The scattering intensity data were processed using the instrumental software to obtain the hydrodynamic diameter (d_h) and size distribution of the scattered data in each sample. The instrument measures the time-dependent fluctuation in the intensity of the light scattered from the particles in solution at a fixed scattering angle. d_h of the reverse micelle was estimated from the intensity autocorrelation function of the time-dependent fluctuation in intensity. d_h is defined as

$$d_h = \frac{k_B T}{3\pi\eta D} \quad (1)$$

where k_B is the Boltzmann constant, η is the viscosity, and D is the translational diffusion coefficient. In a typical size distribution

graph from the DLS measurement, the *x*-axis shows a distribution of size classes in nanometers, while the *y*-axis shows the relative intensity of the scattered light. For viscosity measurements we used a Brookfield DV-II+ Pro (viscometer) at 25 °C. All experiments were carried out at 25 °C. The temperature was maintained as a constant by circulating water through the cell holder using a Laboratory Companion thermostat (RG-0525G). A conductivity meter manufactured by Integrated Electrolife System, having an EP type connector, was used for conductance measurements.

3. RESULTS AND DISCUSSION

3.1. Phase Behavior Study. Phase behavior measurement is essential to study microemulsions. In this work, TX100 was used as the surfactant. The ternary phase diagrams of the $[P_{13}][Tf_2N]$/TX100/benzene system at 25 °C determined in this work by direct observation are illustrated in Figure 1. Since the $[P_{13}]$-$[Tf_2N]$/TX100/benzene microemulsion system is in accord with the percolation theory from the viewpoint of the static percolation model as well as dynamic percolation model, the microstructure investigation can be carried out by electrical conductivity measurement. Above the phase separation boundary curve, the system exists as one phase and the shadow area is the biphasic region. The monophasic region can be divided into different subregions, such as the IL (or polar solvent)-in-oil microemulsion region (IL or polar solvent droplets dispersed in oil), the oil-in-IL (or polar solvent) microemulsion region (oil droplets dispersed in IL or polar solvent), and the bicontinuous region. The subareas can be conveniently located by electrical conductivity measurement. In this work, we determined the subregions by this method. In this case, we have attempted to identify the structural transitions of $[P_{13}][Tf_2N]$/TX100/benzene microemulsion by using insulative benzene as the titration phase. Dilution series of the microemulsions were prepared by fixing weight ratios of $[P_{13}][Tf_2N]$/TX100 (I = 0.10, 0.20, and 0.33) but varying weight fraction of benzene. As the examples, parts a−c of Figure 2 illustrate the dependence of the conductivity on the weight fraction of benzene with weight ratios $[P_{13}][Tf_2N]$/TX100 (I) being 0.10, 20, and 0.33, respectively. The conductivity vs benzene concentration curves were used to locate subregions using the principle and method reported by other authors,[51−53] and the subregions determined are also marked in Figure 1. Figure 2 shows the variation of electrical conductivity k as a function of benzene weight fraction. The initial increase of k, due to the successive increase of conductive O/IL microemulsion droplets, could indicate the formation of O/IL microemulsions. The next nonlinear decrease revealed that the medium underwent a structural transition and became bicontinuous, due to the progressive growth and interconnection of the O/IL microdomains. The third section of the curve, the linear decrease of k, could be interpreted as the consequence of the formation of IL/O microdomains resulting from the partial fusion of clustered inverse microdroplets. The conductivity curves in Figure 2a−c evidently illustrate the presence of three different types of microstructure: O/IL, bicontinuous, and IL/O microemulsions. By repeating the experiment for other samples with different R values, three types of microregions can be determined. The subregions identified were also marked in Figure 1.

3.2. Dynamic Light Scattering and Formation of $[P_{13}][Tf_2N]$/TX100/Benzene Microemulsions. DLS is used to assess whether the ILs are encapsulated by the surfactant to create microemulsions media, because it is a powerful technique to evaluate the formation of these new organized systems. Thus, if the IL is really encapsulated to form microemulsions, the droplets size must increase as the R value increases with a linear tendency (swelling law of microemulsions) as it is well-established for water or polar solvents/surfactant microemulsion systems. This feature can also demonstrate that the IL microemulsions media consist of discrete spherical and noninteracting droplets of ILs stabilized by the surfactant. Deviation from the linearity could be due to several factors, with the most relevant being the droplet−droplet interaction or other microemulsions shape. In the IL/O region described in Figure 1, a series of samples along the dilute line d are measured by DLS at various sample compositions (R = 0.23, 0.46, and 0.69). Figure 3 shows the size distribution of the $[P_{13}][Tf_2N]$-in-benzene microemulsions. The size of aggregates increased from 16 to 58 nm linearly on increasing the [IL]/[TX100] mole ratio from 0.23 to 0.69. The result is similar to those of typical W/O microemulsions,

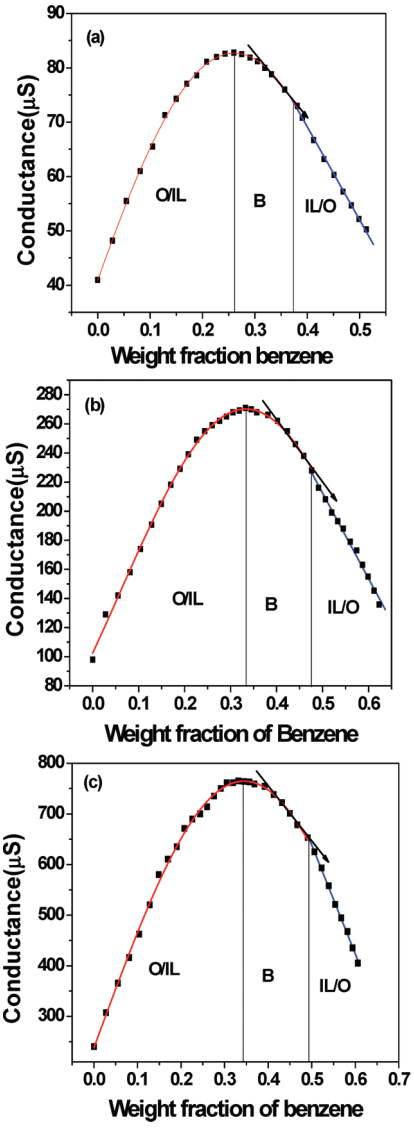

Figure 2. Electric conductivity k of the nonaqueous IL microemulsion as a function of benzene weight content with I = 0.10 (a), 0.20 (b), and 0.40 (c) respectively.

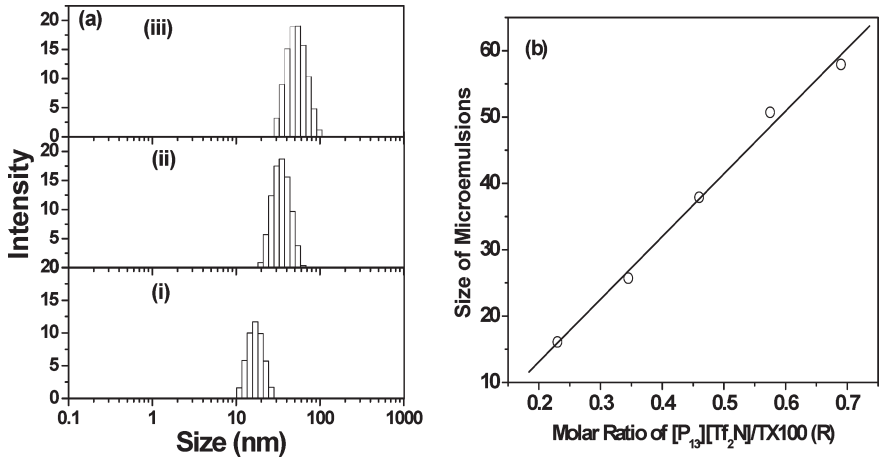

Figure 3. (a) Size distribution of the droplets (measured by DLS) in microemulsions of $[P_{13}][Tf_2N]$/TX100/benzene for R = (i) 0.23, (ii) 0.46, and (iii) 0.69. (b) Diameter values (nm) of the $[P_{13}][Tf_2N]$/TX100/benzene microemulsions at varying R.

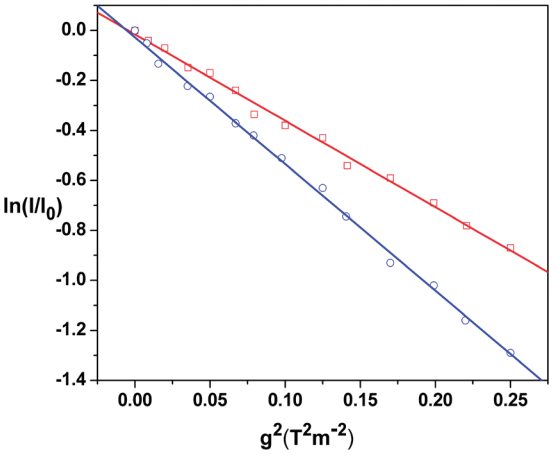

Figure 4. Variation of $\ln(I/I_0)$ versus g^2 for neat $[P_{13}][Tf_2N]$ (□) and $[P_{13}][Tf_2N]$/TX100/benzene microemulsions (R = 0.46; ○).

suggesting the formation of IL/O microemulsions. This regular swelling behavior is consistent with the volume of dispersed nanodomains being directly proportional to the amount of added IL, which is common to many droplet microemulsions, such as sodium bis(2-ethyl-1-hexyl)sulfosuccinate (AOT) stabilized W/O systems.

3.3. Diffusion-Ordered Spectroscopy (DOSY) NMR Study. We have used pulsed-field gradient spin−echo NMR (PFGSE NMR) technique to determine the diffusion coefficient of $[P_{13}]^+$ cation in neat $[P_{13}][Tf_2N]$ and $[P_{13}][Tf_2N]$ in microemulsion (R = 0.46). Self-diffusion coefficients were obtained by varying the gradient strength (g) while keeping the gradient pulse length (δ) and the gradient pulse interval constant within each experimental run. The data were fitted according to the Stejskal−Tanner equation:

$$\frac{I}{I_0} = \exp\left[-Dq^2\left(\Delta - \frac{\delta}{3}\right)\right] \qquad (2)$$

where I and I_0 are the signal intensities in the presence and absence of the applied field gradient, respectively, $q = \gamma g\delta$ is the so-called scattering vector, γ is the gyromagnetic ratio of the observed nucleus, $t = (\Delta - \delta/3)$ is the diffusion time, Δ is the delay between the encoding and decoding gradients, and D is the self-diffusion coefficient to be extracted.[54] In our experiments, δ and Δ were fixed at 1 and 1 ms, respectively. The variation of $\ln(I/I_0)$ versus g^2 is shown in Figure 4, and the diffusion coefficient of $[P_{13}]^+$ cation is calculated by the slope of the plot. The diffusion data for the $[P_{13}]^+$ cation are shown in Table 1. The diffusion coefficient of $[P_{13}]^+$ cation in neat $[P_{13}][Tf_2N]$ and $[P_{13}][Tf_2N]$ containing microemulsions (R = 0.46) was found to be 3.10×10^{-10} and 5.41×10^{-10} m^2 s^{-1}, respectively. The diffusion coefficient, D, can be related to the viscosity of the solution, η, by the well-known Stokes−Einstein equation on the basis of hydrodynamic model that a solute sphere moves through a continuum fluid.

$$D = \frac{k_B T}{6\pi r\eta} \qquad (3)$$

The viscosity neat $[P_{13}][Tf_2N]$ and $[P_{13}][Tf_2N]$-containing microemulsions (R = 0.46) was found to be 51 and 4 cP, respectively. In our case the viscosity decreases, almost by a factor of ~13 times on going from neat $[P_{13}][Tf_2N]$ to $[P_{13}][Tf_2N]$-containing microemulsions (R = 0.46). D of $[P_{13}][Tf_2N]$ in microemulsions (R = 0.46) is 1.74 times faster compared to neat $[P_{13}][Tf_2N]$. Thus, if the IL is not encapsulated by the surfactant to form

Table 1. Steady-State Absorption and Emission Maxima of C-153 and C-480 in Neat $[P_{13}][Tf_2N]$ and in $[P_{13}][Tf_2N]$/TX100/Benzene Microemulsions

system	$^{max}\lambda_{abs}$ (nm)	$^{max}\lambda_{em}$ (nm)
TX100/Benzene/C-153	410	501
$[P_{13}][Tf_2N]$/TX100/benzene (R = 0.23) C153	418	511
$[P_{13}][Tf_2N]$/TX100/benzene (R = 0.46) C153	420	513
$[P_{13}][Tf_2N]$/TX100/benzene (R = 0.69) C153	421	515
neat $[P_{13}][Tf_2N]$ + C153	424	523
TX100/benzene/C-480	377	443
$[P_{13}][Tf_2N]$/TX100/benzene (R = 0.23) C-480	380	454
$[P_{13}][Tf_2N]$/TX100/Benzene (R = 0.46) C-480	381	454
$[P_{13}][Tf_2N]$/TX100/benzene (R = 0.69) C-480	382	455
neat $[P_{13}][Tf_2N]$ + C480	385	460

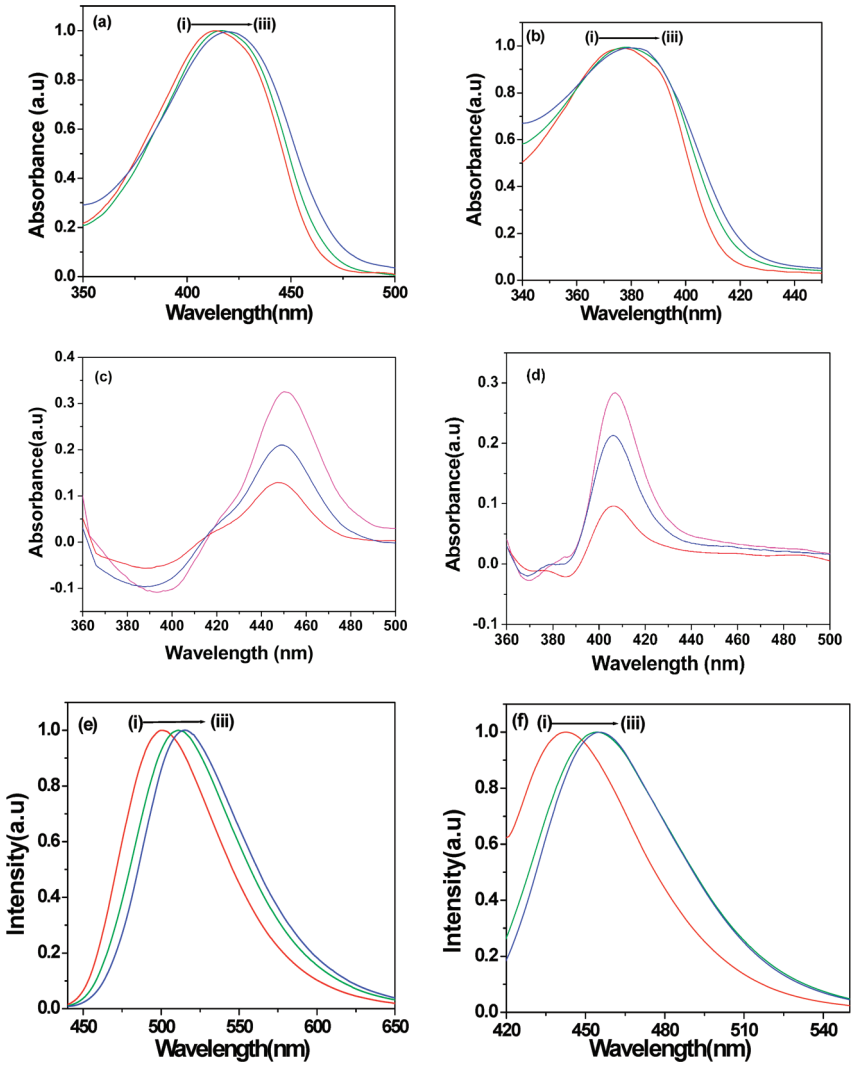

Figure 5. (a, b) Absorption spectra of C153 and C480 in (i) 0.5 M TX100 in benzene and $[P_{13}][Tf_2N]$/TX100/benzene microemulsions and R = (ii) 0.23 and (iii) 0.69, respectively. (c) Difference spectra between C-153 in benzene and that of C-153 in (i) benzene with TX100 (red line), (ii) benzene with TX100 and ionic liquid (R = 0.23) (blue line), and (iii) benzene with TX100 and ionic liquid (R = 0.69) (pink line), respectively. (d) Difference spectra between C-480 in benzene and that of C-480 in (i) benzene with TX100 (red line), (ii) benzene with TX100 and ionic liquid (R = 0.23) (blue line), and (iii) benzene with TX100 and ionic liquid (R = 0.69) (pink line), respectively. (e, f) Emission spectra of C-153 and C-480 in (i) 0.5 M TX100 in benzene and $[P_{13}][Tf_2N]$/TX100/benzene microemulsions and R = (ii) 0.23 and (iii) 0.69, respectively.

microemulsions, then the diffusion coefficient of $[P_{13}][Tf_2N]$ in microemulsions is also decreases 13 times as the viscosity decreases of $[P_{13}][Tf_2N]$ containing microemulsions systems compared to $[P_{13}][Tf_2N]$. Hence diffusion of $[P_{13}][Tf_2N]$ clearly indicates that $[P_{13}][Tf_2N]$ encapsulated by the TX100 surfactant to form microemulsions. The estimated value of the diffusion constant for the nanodroplet of the IL microemulsion at R = 0.46 having the size of 38 nm (from DLS study) and viscosity 4 cP is $D_{droplet} \sim 2.80 \times 10^{-12}$ m^2 s^{-1}. This value is ~200 times lesser than the measured diffusion constant $\sim 5.41 \times 10^{-10}$ m^2 s^{-1} of ILs present in the microemulsions. Hence the diffusion of the nanodroplet of the IL microemulsion cannot contribute in the measured diffusion constant of IL present in the microemulsions.

3.4. Steady-State Absorption and Emission Spectra. The absorption and emission spectra of C153 and C480 were taken in benzene and in microemulsions. The absorption and emission spectra of C153 and C480 are illustrated in Figure 5a,b,e,f, respectively. The absorption and emission maxima are listed in Table 1. The emission maxima of the probes C153 and C480 in benzene are 482 and 423 nm and in $[P_{13}][Tf_2N]$ are 523 and 460 nm, respectively. On addition of TX100 to a solution of C153 in benzene emission maxima shifted from 482 to 501 nm. In the case of C480 emission maxima shifted from 423 to 443 nm on addition of TX100 to a solution of C480 in benzene. This marked red shift of emission maxima of both the probes indicates the transfer of probe molecules from bulk benzene to the interior of the TX100 reverse micelle. On addition of RTIL ($[P_{13}][Tf_2N]$) to the TX100/benzene mixture, the emission maxima further red-shifted (Figure 5e,f). The red shift suggests that the probe molecules are located inside the polar core of the microemulsions. The absorbance of both probes at the red end side of the absorption spectra increases with the gradual addition of $[P_{13}][Tf_2N]$ to the TX100/benzene mixture. This indicates that a substantial number of probe molecules migrate from the bulk benzene to the ionic liquids core of the microemulsions.

dx.doi.org/10.1021/jp110896w |J. Phys. Chem. B 2011, 115, 2322–2330

To find the location of the probe, we have constructed the difference in absorption spectra of C-153 and C-480 in benzene without TX100 and with TX100 and ionic liquid. In benzene, C-153 exhibits a peak around 407 nm. On addition of TX100 and subsequently ionic liquid in benzene, the absorbance of the peak around 407 nm decreases and there is an increase in optical density around 450 nm. The difference of the absorbance spectra of C-153 in benzene with TX100 and ionic liquid and that of C-153 in benzene without TX100 and ionic liquid exhibits a negative absorbance around 407 nm, and there is a distinct peak above 450 nm. The depletion of the population of C-153 on addition of ionic liquid at 407 nm clearly indicates that the population of C-153 at 407 nm decreases. On the other hand, the increase of optical density above 450 nm indicates that the probe molecules are shifted toward the polar region of the microemulsions. The representative difference in absorbance spectra of C-153 and C-480 in ionic liquid microemulsions is shown in Figure 5c,d, respectively. The difference in absorption spectra in the case of C-480 in ionic liquid microemulsions is similar.

3.5. Time-Resolved Studies. To study solvent relaxation dynamics, we collected the time-resolved decays monitored at different wavelengths for all of the systems. The decays at the red edge of the emission spectra were preceded by a growth in the fraction of nanosecond time scale while decays at the short wavelengths are fast. The wavelength-dependent behavior of temporal decays of C-480 clearly indicates that solvent relaxation is taking place in these systems. The time-resolved emission spectra (TRES) were constructed using the procedure of Fleming and Maroncelli.[55] The TRES at a given time t, $S(\lambda;t)$, is obtained by the fitted decays, $D(t;\lambda)$, by relative normalization to the steady-state spectrum $S_0(\lambda)$, as follows.

$$S(\lambda;t) = D(\lambda;t)\frac{S_0(\lambda)}{\int_0^\infty D(\lambda;t)\,dt} \quad (4)$$

Each TRES was fitted by a log-normal line shape function, which is defined as

$$g(\nu) = g_0 \exp\left[-(\ln 2)\left(\frac{\ln[1+2b(\nu-\nu_p)]/\Delta}{b}\right)^2\right] \quad (5)$$

where g_0, b, ν_p, and Δ are the peak height, asymmetric parameter, peak frequency, and width parameter, respectively. We have obtained the peak frequency from the log-normal fitting of TRES. The solvation dynamics was monitored by the solvent response function defined as

$$C(t) = \frac{\nu(t)-\nu(\infty)}{\nu(0)-\nu(\infty)} \quad (6)$$

where $\nu(0)$, $\nu(t)$, and $\nu(\infty)$ are the peak frequencies at time 0, t, and infinity, respectively. The solvent response function $(C(t))$ was fitted to a biexponential decay function

$$C(t) = a_1 \exp^{(-t/\tau_1)} + a_2 \exp^{(-t/\tau_2)} \quad (7)$$

where τ_1 and τ_2 are the two relaxation times with amplitude a_1 and a_2, respectively.

Before describing the solvent relaxation results in these microemulsions, we will discuss some distinct features of solvation dynamics in neat RTILs. It should be noted that solvation dynamics in RTILs are totally different from other polar solvents such as methanol and acetonitrile, etc.[56,57] Solvation in RTILs takes place due to the motion of ions around an excited dye, while in water, methanol, and acetonitrile, i.e., in polar solvents, solvation takes place as the solvent molecules reorient themselves around an excited dye. Recent ultrafast studies suggest the differences are less striking than originally thought.[41] Chapman and Maroncelli[58] showed that ionic solvation is slower compared to the pure solvent and dependent on the viscosity of the medium. Samanta and co-workers observed biphasic solvation dynamics in different RTILs.[59] They ascribed the fast component to the motion of the anions, and the slow component is ascribed to the collective motions of both cation and anions, respectively. Petrich and co-workers observed that the polarizability of the cation is responsible for the fast component.[60] To understand the solvation process in RTILs, a number of simulation studies have been performed.[61−63] One of the early studies by Shim et al. attributes the fast component of the dynamics to the translational motion of the anion and the slow component to the overall diffusional motion of the cation and anion.[61] Kobrak and Znamenskiy, on the other hand, assigned the ultrafast component of the dynamics to the collective cation−anion motion.[62] Later, Shim et al. suggested that ultrafast dynamics is dependent on the local density of the ions near the probe molecules.[63] Kashyap and Biswas[64] noted the dipolar nature of the imidazolium cations and thought that the dipole−dipole interactions might play an important role in the solvent stabilization of the fluorescent state of the dipolar molecules and, hence, can contribute to the dynamic Stokes shift.

To comprehend the solvation dynamics results, a thorough understanding of the microemulsions structure and location of the probe within the microemulsions are necessary. From UV, the fluorescence study showed that substantial numbers of probe molecule reside in the core of the microemulsions. In this article we report solvation times of C-480 and C-153 in neat $[P_{13}][Tf_2N]$ and in $[P_{13}][Tf_2N]$/TX100/benzene microemulsions. The average solvation time of C-153 in neat $[P_{13}][Tf_2N]$ is 0.46 ns with time constants of 160 and 530 ps with relative contribution of the fast and slow components being 20 and 80%, respectively (Figure 6c). The solvent relaxation time of C-480 in neat $[P_{13}][Tf_2N]$ is 0.47 ns which consists of two components with time constants of 350 and 920 ps with relative contributions of the fast and slow components being 78 and 22%, respectively (Figure 6d). These time constants are totally different from the time constants observed in microemulsions (Figure 6a). When we incorporated these solvents inside the microemulsion core, their solvent responses were ~10 times retarded. This is due to the nanocage confinement of the solvent inside the microemulsions core. For both probes we have observed bimodal solvation dynamics in these $[P_{13}][Tf_2N]$/TX100/benzene microemulsions at different R values. In the case of C153 at R = 0.23 the value of the fast component is 0.65 ns and that of the slow component is 16.90 ns with relative contributions of 68 and 32%, respectively. With gradual increasing in R (i.e., gradual RTIL loading in microemulsions), the fast components became faster, whereas the slow components decrease marginally. We also observed an increase in the relative contribution of the faster component and a decrease in relative contribution of the slower component. In the case of C-153 the fast and slow components of solvent relaxation are decreased from 0.65 to 0.57 ns and from 16.90 to 16.21 ns, respectively, with an increase in R from 0.23 to 0.69 (Table 2). The changes in the relative contribution of the components and decrease in both components of solvation time with increases in R lead to a decrease in the average solvation

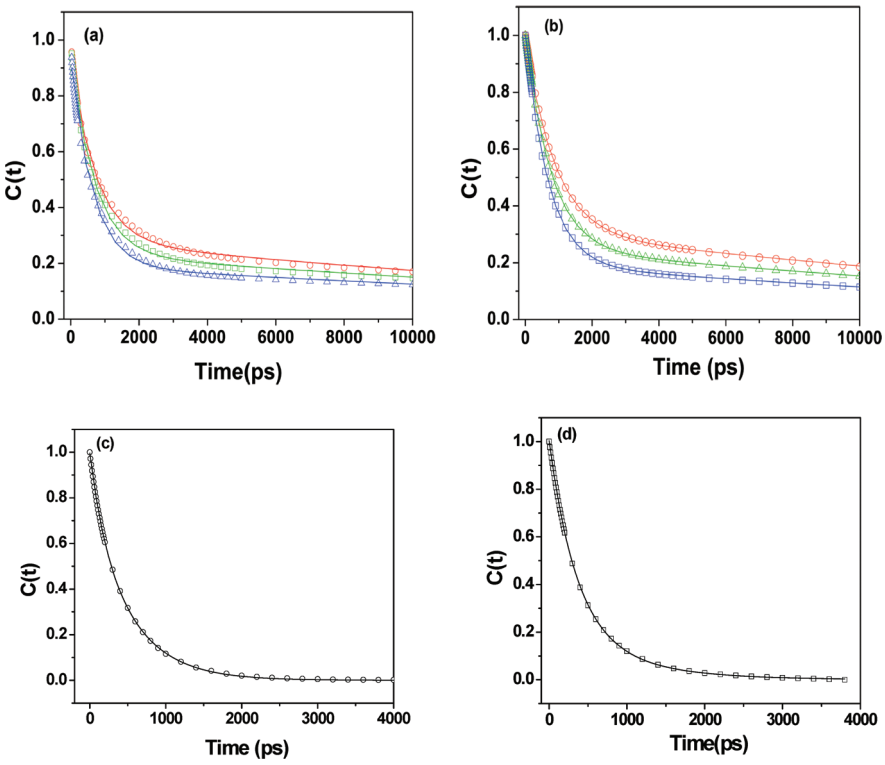

Figure 6. (a, b) Decay of solvent correlation function $C(t)$ of C153 and C480 in $[P_{13}][Tf_2N]$/TX100/benzene microemulsions at R = (i) 0.23 (○), (ii) 0.46 (△), and (iii) 0.69 (□), respectively. (c, d) Decay of solvent correlation function $C(t)$ of C153 (○) and C480 (□), respectively, in neat $[P_{13}][Tf_2N]$.

Table 2. Decay Parameters of Solvent Correlation Function $C(t)$ of C-153 and C-480 Probes in Neat $[P_{13}][Tf_2N]$ and in $[P_{13}][Tf_2N]$/TX100/Benzene Microemulsions

system	α_1	α_2	τ_1 (ns)	τ_2 (ns)	τ_{av} (ns)	size (nm)
$[P_{13}][Tf_2N]$/TX100/benzene (R = 0.23) C153	0.68	0.32	0.65	16.90	5.85	16
$[P_{13}][Tf_2N]$/TX100/benzene (R = 0.46) C153	0.72	0.28	0.63	16.85	5.17	38
$[P_{13}][Tf_2N]$/TX100/benzene (R = 0.69) C153	0.77	0.23	0.57	16.21	4.36	58
Neat $[P_{13}][Tf_2N]$ + C153	0.20	0.80	0.16	0.53	0.46	
$[P_{13}][Tf_2N]$/TX100/benzene (R = 0.23) C480	0.66	0.34	0.80	14.78	5.56	16
$[P_{13}][Tf_2N]$/TX100/benzene (R = 0.46) C480	0.72	0.28	0.72	14.70	4.66	38
$[P_{13}][Tf_2N]$/TX100/benzene (R = 0.69) C480	0.79	0.21	0.65	13.88	3.43	58
Neat $[P_{13}][Tf_2N]$ + C480	0.78	0.22	0.35	0.92	0.47	

time. The solvents relaxation in RTILs depends on translational motions of ions of the RTILs. There are two types of RTIL present in the microemulsions that are in different environments, near and apart from surfactants headgroup. The RTILs present near the surfactant headgroup, i.e., at the interfacial regions, encounter a restricted environment compared to the RTILs in the core of the microemulsions. So the slow component arises due to RTIL molecules present at the interfacial regions of the microemulsions. The RTIL molecules being apart from surfactants molecules contribute to the fast component of solvation dynamics. At low RTIL loading, i.e., lower R values, most of the RTIL molecules will be involved in solvating the surfactant and forming ion−dipole interaction with ionic liquid and surfactant headgroup. As more RTILs are added to the system, RTIL begins to form a bulk-like pool where the RTIL is less restricted compared to RTIL present at the interfacial region. As the R values increases, the proportion of ionic liquid in the interfacial regions decreases and the proportion of ionic liquid in the core of the microemulsions increases, which leads to an increase in the diffusional motion of the ions and decreases the slow and fast component values of the solvation dynamics, consequently decreasing the average solvation time. We also observed that, at higher R values, the relative contribution of the slow component of the solvation dynamics decreases which indicated that more C-153 probe molecules reside at the core of the microemulsions at higher R values and therefore decrease the average solvation time.

In the case of C-480 the fast and slow components of solvation time are decreasing from 0.80 to 0.65 ns and from 14.78 to 13.88 ns, respectively, with an increase in the R value from 0.23 to 0.69. With the increase in R the relative contribution of the fast component is gradually increasing. The decrease of the relative contribution of the slow components, the increase in the contribution of the fast components, and the decrease in the time

contants of both of the components lead to faster solvation dynamics when R values increase. The average solvation time of C-480 at R = 0.23 is 5.56 ns, consisting of time constants of the fast component of 800 ps (with relative contribution of 66%) and the slow component of 14.80 ns (with relative contribution of 34%). At R = 0.69 the average solvation time of C-480 is 3.43 ns with time constants of the fast component being 650 ps with relative contribution of 79% and the slow component being 13.88 ns with the relative contribution of 21% (Table 2). Thus the slow dynamics in microemulsion is essentially the dynamics inside the core of the microemulsions. Figure 5d indicates that with the increase in RTIL loading more C-480 molecules have been shifted toward the pool of the microemulsions, so the relative contribution of the slow component decreases; therefore the average solvation time decreases. For both probes with an increase in R the relative contribution of the fast components increases and the relative contribution of the slow components decreases, so the average solvation time decreases (Figure 6a,b). Previous studies carried out by our group showed that in $[N_{3111}][Tf_2N]$/TX100/cyclohexane microemulsions a change in solvation time with varying R was not that significant compared with the present study.[17] This may be due to the fact that the size variation was not large, for example, from 10 to 23 nm upon increasing R value from 0.08 to 0.30 compared the present study where the size variation is large from 16 to 58 nm upon increasing R value from 0.23 to 0.69.

4. CONCLUSIONS

In summary, microemulsions consisting of $[P_{13}][Tf_2N]$, surfactant TX-100, and benzene were prepared and the phase behavior of the ternary system was investigated. The $[P_{13}][Tf_2N]$-in-benzene (IL/O), bicontinuous, and benzene-in-$[P_{13}][Tf_2N]$ (O/IL) microregions of the nonaqueous RTIL microemulsions were initially identified by traditional electrical conductivity measurements on the basis of percolation theory. Diffusion coefficient of neat $[P_{13}][Tf_2N]$ and $[P_{13}][Tf_2N]$ in microemulsions has been measured by using DOSY NMR which indicates ionic liquid containing microemulsions is formed. Steady-state and time-resolved fluorescence spectroscopy have been used to investigate the structure and dynamical behavior of $[P_{13}][Tf_2N]$/TX100/benzene microemulsions with variation of ionic liquid content. The motions of the ions of RTILs are responsible for the slow solvation dynamics. With the increase in RTIL loading more probes molecules has been shifted toward the pool of the microemulsions where the motions of RTIL are faster compared to the interfacial regions RTIL; consequently the solvent relaxation are faster.

AUTHOR INFORMATION

Corresponding Author

*E-mail: nilmoni@chem.iitkgp.ernet.in. Fax: 91-3222-255303.

ACKNOWLEDGMENT

N.S. is thankful to the Department of Science and Technology (DST) and the Board of Research in Nuclear Sciences (BRNS), Government of India, for generous research grants. R.P., C.G., and V.G.R. are thankful to CSIR for research fellowships. S.S. is thankful to BRNS for SRF.

REFERENCES

(1) (a) Welton, T. *Chem. Rev.* **1999**, *99*, 2071. (b) Parvulescu, V. I.; Hardacre, C. *Chem. Rev.* **2007**, *107*, 2615. (c) Haumann, M.; Riisager, A. *Chem. Rev.* **2008**, *108*, 1474. (d) Plechkova, N. V.; Seddon, K. R. *Chem. Soc. Rev.* **2008**, *37*, 123. (e) Rantwijk, F. V.; Sheldon, R. A. *Chem. Rev.* **2007**, *107*, 2757.

(2) Wasserscheid, P.; Keim, W. *Angew. Chem., Int. Ed.* **2000**, *39*, 3772.

(3) Seddon, K. R. *J. Chem. Technol. Biotechnol.* **1997**, *68* (1), 351.

(4) Hagiwara, R.; Ito, Y. *J. Fluorine Chem.* **2000**, *105*, 221.

(5) Huddleston, J. G.; Willauer, H. W.; Swatloski, R. P.; Visser, A. E.; Rogers, R. D. *Chem. Commun. (Cambridge, U. K.)* **1998**, 1765.

(6) Broker, G. A.; Rogers, R. D. *Green Chem.* **2001**, *3*, 156.

(7) Earle, M. J.; Seddon, K. R.; McCormac, P. B. *Green Chem.* **2000**, *2*, 261.

(8) Wasserscheid, P.; Welton, T. *Ionic Liquids in Synthesis*; Wiley-VCH: Weinheim, Germany, 2002.

(9) Dupont, J.; de Souza, R. F.; Suarez, P. A. Z. *Chem. Rev.* **2002**, *102*, 3667.

(10) Cole, A. C.; Jensen, J. L.; Ntai, I.; Tran, K. L. T.; Weaver, K. J.; Forbes, D. C., Jr.; Davis, J. H. *J. Am. Chem. Soc.* **2002**, *124*, 5962.

(11) Brown, R. A.; Pollet, P.; McKoon, E.; Eckert, C. A.; Liotta, C. L.; Jessop, P. G. *J. Am. Chem. Soc.* **2001**, *123*, 1254.

(12) (a) Solans, C.; Kunieda, H.; Industrial Application of Microemulsions. *Surfactant Science Series*; Dekker: New York, 1997; p 66. (b) Tadros, T. F.; *Applied Surfactant—Principle and Applications*; Wiley-VCH: Weinheim, Germany, 2005. (c) Somasundaran, P. *Encyclopedia of Surface and Colloid Science*; CRC Press: Boca Raton, FL, 2006. (d) Johnston, K. P.; Harrison, K. L.; Clarke, M. J.; Howdle, S. M.; Heitz, M. P.; Bright, F. V.; Carlier, C.; Randolph, T. W. *Science* **1996**, *271*, 624. (e) Eastoe, J.; Gold, S.; Rogers, S.; Wyatt, P.; Steytler, D. C.; Gurgel, A.; Heenan, R. K.; Fan, X.; Beckman, E. J.; Enick, R. M. *Angew. Chem., Int. Ed.* **2006**, *45*, 3675. (f) Liu, Y.; Jessop, P. G.; Cunningham, M.; Eckert, C. A.; Liotta, C. L. *Science* **2006**, *313*, 958. (g) Ohde, H.; Wai, C. M.; Kim, H.; Kim, J.; Ohde, M. *J. Am. Chem. Soc.* **2002**, *124*, 4540. (h) Schubert, K. V.; Lusvardi, K. M.; Kaler, E. W. *Colloid Polym. Sci.* **1996**, *274*, 875. (i) Spiro, M.; de Jesus, D. M. *Langmuir* **2000**, *16*, 2464. (j) Bonini, M.; Bardi, U.; Berti, D.; Neto, C.; Baglioni, P. *J. Phys. Chem. B* **2002**, *106*, 6178. (k) Lv, F. F.; Zheng, L. Q.; Tung, C. *Int. J. Pharm.* **2005**, *301*, 237.

(13) Fletcher, K. A.; Pandey, S. *Langmuir* **2004**, *20*, 33.

(14) Cheng, S.; Zhnag, J.; Zhang, Z.; Han, B. *Chem. Commun. (Cambridge, U. K.)* **2007**, 2497.

(15) Gao, Y.; Han, S.; Han, B.; Li, G.; Shen, D.; Li, Z.; Du, J.; Hou, W.; Zhang, G. *Langmuir* **2005**, *21*, 5681.

(16) Eastoe, J.; Gold, S.; Rogers, S. E.; Paul, A.; Welton, T.; Heenan, R. K.; Grillo, I. *J. Am. Chem. Soc.* **2005**, *127*, 7302.

(17) Pramanik, R.; Sarkar, S.; Ghatak, C.; Rao, V. G.; Setua, P.; Sarkar, N. *J. Phys. Chem. B* **2010**, *114*, 7579.

(18) Aki, S. N. V. K.; Brennecke, J. F.; Samanta, A. *Chem. Commun. (Cambridge, U. K.)* **2001**, 413.

(19) Muldoon, M. J.; Gordon, C. M.; Dunkin, I. R. *J. Chem. Soc., Perkin Trans. 2* **2001**, *2*, 433.

(20) Reichardt, C. *Green Chem.* **2005**, *7*, 339.

(21) Carmichael, A. J.; Seddon, K. R. *J. Phys. Org. Chem.* **2000**, *13*, 591.

(22) Fletcher, K. A.; Pandey, S. *J. Phys. Chem. B* **2003**, *107*, 13532.

(23) Fletcher, K. A.; Baker, S. N.; Baker, G. A.; Pandey, S. *New J. Chem.* **2003**, *27*, 1706.

(24) Baker, S. N.; Baker, G. A.; Bright, F. V. *Green Chem.* **2002**, *4*, 165.

(25) Pandey, S.; Fletcher, K. A.; Baker, S. N.; Baker, G. A. *Analyst* **2004**, *129*, 569.

(26) Chakrabarty, D.; Chakraborty, A.; Hazra, P.; Seth, D.; Sarkar, N. *Chem. Phys. Lett.* **2004**, *397*, 216.

(27) Santhosh, K.; Samanta, A. *J. Phys. Chem. B* **2010**, *114*, 9195.

(28) Santhosh, K.; Banerjee, S.; Rangaraj, N.; Samanta, A. *J. Phys. Chem. B* **2010**, *114*, 1967.

(29) Chakrabarty, D.; Hazra, P.; Chakraborty, A.; Seth, D.; Sarkar, N. *Chem. Phys. Lett.* **2003**, *381*, 697.

(30) Shim, Y.; Jeong, D.; Manjari, S.; Choi, M. Y.; Kim, H. J. *Acc. Chem. Res.* **2007**, *40*, 1130.

(31) Kashyap, H. K.; Biswas, R. *J. Phys. Chem. B* **2008**, *112*, 12431.
(32) Kashyap, H. K.; Biswas, R. *J. Phys. Chem. B* **2010**, *114*, 254.
(33) (a) Saha, S.; Mandal, P. K.; Samanta, A. *Phys. Chem. Chem. Phys.* **2004**, *6*, 3106. (b) Samanta, A. *J. Phys.Chem. Lett.* **2010**, *1*, 1557.
(34) Chowdhury, P. K.; Halder, M.; Sanders, L.; Calhoun, T.; Anderson, J. L.; Armstrong, D. W.; Song, X.; Petrich, J. W. *J. Phys. Chem. B* **2004**, *108*, 10245.
(35) Lang, B.; Angulo, G.; Vauthey, E. *J. Phys. Chem. A* **2006**, *110*, 7028.
(36) Ingram, J. A.; Moog, R. S.; Ito, N.; Biswas, R.; Maroncelli, M. *J. Phys. Chem. B* **2003**, *107*, 5926.
(37) Ito, N.; Arzhantsev, S.; Heitz, M.; Maroncelli, M. *J. Phys. Chem. B* **2004**, *108*, 5771.
(38) Arzhantsev, S.; Ito, N.; Heitz, M.; Maroncelli, M. *Chem. Phys. Lett.* **2003**, *381*, 278.
(39) Castner, E. W., Jr.; Wishart, J. F.; Shirota, H. *Acc. Chem. Res.* **2007**, *40*, 1217.
(40) (a) Karmakar, R.; Samanta, A. *J. Phys. Chem. A* **2002**, *106*, 6670. (b) Karmakar, R.; Samanta, A *J. Phys. Chem. A* **2003**, *107*, 7340. (c) Samanta, A. *J. Phys. Chem. B* **2006**, *110*, 13704. (d) Mandal, P. K.; Paul, A.; Samanta, A. *J. Photochem. Photobiol. A* **2006**, *182*, 113.
(41) Jin, H.; Baker, G. A.; Arzhantsev, S.; Dong, J.; Maroncelli, M. *J. Phys. Chem. B* **2007**, *111*, 7291.
(42) (a) Funston, A. M.; Fadeeva, T. A.; Wishart, J. F.; Castner, E. W., Jr. *J. Phys. Chem. B.* **2007**, *111*, 4963. (b) Dhumal, N. R.; Kim, H. J.; Kiefer, J. *J. Phys. Chem. A* **2009**, *113*, 10397. (c) Shirota, H.; Castner, E. W., Jr. *J. Phys. Chem. A* **2005**, *109*, 9388. (d) Kobrak, M. N. *J. Chem. Phys.* **2006**, *125*, 064502. (e) Jeong, D.; Shim, Y.; Choi, M. Y.; Kim, H. J. *J. Phys. Chem. B* **2007**, *111*, 4920. (f) Bhargava, B. L.; Balasubramanian, S. *J. Chem. Phys.* **2006**, *125*, 219901. (g) Huang, X. H.; Margulis, C. J.; Li, Y. H.; Berne, B. J. *J. Am. Chem. Soc.* **2005**, *127*, 17842. (h) Liu, X.; Zhou, G.; Zhang, S.; Wu, G.; Yu, G. *J. Phys. Chem. B* **2007**, *111*, 5658. (i) Ghatee, M. H.; Ansari, Y. *J. Chem. Phys.* **2007**, *126*, 154502.
(43) Chakrabarty, D.; Chakraborty, A.; Seth, D.; Sarkar, N. *J. Phys. Chem. A* **2005**, *109*, 1764.
(44) Paul, A.; Samanta, A. *J. Phys. Chem. B* **2008**, *112*, 947.
(45) Baker, S. N.; Baker, G. A.; Munson, C. A; Chen, F; Bukowski, E. J.; Cartwright, A. N.; Bright, F. V. *Ind. Eng. Chem. Res.* **2003**, *42*, 6457.
(46) Adhikari, A.; Sahu, K.; Dey, S.; Ghosh, S.; Mandal, U.; Bhattacharyya, K. *J. Phys. Chem. B* **2007**, *111*, 12809.
(47) Mukherjee, P.; Crank, J. A.; Halder, M.; Armstrong, D. W.; Petrich, J. W. *J. Phys. Chem. A* **2006**, *110*, 10725.
(48) Mandal, P. K.; Sarkar, M.; Samanta, A. *J. Phys. Chem. A* **2004**, *108*, 9048.
(49) Hu, Z.; Margulis, C. J. *Acc. Chem. Res.* **2007**, *40*, 1097.
(50) (a) Chakrabarty, D.; Chakraborty, A.; Seth, D.; Hazra, P.; Sarkar, N. *Chem. Phys. Lett.* **2004**, *397*, 469. (b) Hazra, P.; Chakrabarty, D.; Chakraborty, A.; Sarkar, N. *Chem. Phys. Lett.* **2003**, *38*, 271.
(51) Clausse, M.; Peyrelasse, J.; Hell, J.; Boned, C.; Lagourette, B. *Nature* **1981**, *293*, 636.
(52) Raj, W. R. P.; Sasthav, M.; Cheung, M. H. *Langmuir* **1991**, *7*, 2586.
(53) Kirkpartrick, S. *Phys. Rev. Lett.* **1971**, *27*, 1722.
(54) Tanner, J. E.; Stejskal, E. O. *J. Chem. Phys.* **1968**, *49*, 1768.
(55) Maroncelli, M.; Fleming, G. R. *J. Chem. Phys.* **1987**, *86*, 6221.
(56) (a) Vajda, S.; Jimenez, R.; Rosenthal, S. J.; Fidler, V.; Fleming, G. R.; Castner, E. W., Jr. *J. Chem. Soc., Faraday Trans.* **1995**, *91*, 867. (b) Kahlow, M. A.; Kang, T. J.; Barbara, P. F. *J. Chem. Phys.* **1988**, *88*, 2372.
(57) (a) Maroncelli, M. *J. Mol. Liq.* **1993**, *57*, 1. (b) Horng, M. L.; Gardecki, J. A.; Papazyan, A.; Maroncelli, M. *J. Phys. Chem.* **1995**, *99*, 17311.
(58) Chapman, C. F.; Maroncelli, M. *J. Phys. Chem.* **1991**, *95*, 9095.
(59) Karmakar, R.; Samanta, A. *J. Phys. Chem. A* **2002**, *106*, 4447.
(60) Headley, L. S.; Mukherjee, P.; Anderson, J. L.; Ding, R.; Halder, M.; Armstrong, D. W.; Song, X.; Petrich, J. W. *J. Phys. Chem. A* **2006**, *110*, 9549.
(61) Shim, Y.; Duan, J. S.; Choi, M. Y.; Kim, H. J. *J. Chem. Phys.* **2003**, *119*, 6411.
(62) (a) Kobrak, M. N.; Znamenskiy, V. *Chem. Phys. Lett.* **2004**, *395*, 127. (b) Znamenskiy, V.; Kobrak, M. N. *J. Phys. Chem. B* **2004**, *108*, 1072.
(63) Shim, Y.; Choi, M. Y.; Kim, H. J. *J. Chem. Phys.* **2005**, *122*, 044511.
(64) (a) Kashyap, H. K.; Biswas, R. *J. Phys. Chem. B* **2008**, *112*, 12431. (b) Kashyap, H. K.; Biswas, R. *J. Phys. Chem. B* **2010**, *114*, 254.